Multi-Disciplinary Analysis of a Strip Stabilizer using Body-Fluid-Structure Interaction Simulation and Design of Experiments (DOE)

M. Mohammadi Amin[†] and A. Kiani

Aerospace Research Institute, Tehran 1465774111, Iran

†*Corresponding Author Email: mmohammadi@ari.ac.ir*

ABSTRACT

The stability of aerospace vehicles is one of the concerning subjects for aerospace engineers and researchers and there are different solutions for the stabilization purpose including rigid and flexible stabilizers use. Design and analysis of such systems generally need multi-disciplinary analysis tools and also efficient design strategies. The first goal of this paper is to develop a computational framework for the simulation of body-fluid-structure interactions (BFSI) due to the oscillations of a flexible stabilizer connected to the end of body. For analyzing fluid-structure interactions, an iterative partitioned coupling algorithm is utilized. With combining a dynamic simulation tool for body motions, the ultimate multidisciplinary framework is arranged. As the second goal of the work, for the sensitivity analysis and also constructing a cost-efficient basis for parametric study, the design of experiments (DOE) methodology is implemented. The proficiency and efficiency of computations is evaluated with the results obtained in a variety stabilizing conditions and various strip characteristics such as length, width, and bending stiffness. The results of different simulations shows that the proposed framework is capable to capture the multi-physic nature of the problem with reasonable cost, especially useful for frequent analyses needed during product design and development loops.

NOMENCLATURE

A	area	μ	dynamic viscosity
E	module of elasticity	μ	dynamic viscosity
h	angular momentum	U, V, W	linear Velocity
I	moment of inertia	W_i	natural modes
M	moment	w	transverse displacement
P	pressure		
P, Q, R	angular velocity	$\eta_i(t)$	generalized coordinates
$Q_i(t)$	generalized forces	ρ	density
T	temperature	ω	angular velocity

1. INTRODUCTION

In order to ensure the stability of some of the flying bodies, concerning configuration and volume constraints, usually flexible retractable stabilizers are used. Samples of these stabilizers are strips that in addition to providing dynamic stability, occupy a small volume and space. Of course, the analysis and design of the strip should be done correctly to provide the dynamic stability of the body; otherwise, the body will be unstable and its oscillations will lead to the failure of the mission. In this paper, the stability of Sub-orbital Re-entry Capsule that has been used for carrying live organism in the Aerospace Research Institute (ARI), is investigated and the effect of the stabilizing strip on this reentry capsule is analyzed (https://www.ari.ac.ir). The reason for using the strip in this capsule is that before the parachute is opened and the speed of the vehicle is reduced (Fig.

1, stage 2), it is necessary to reach initial stability and its rotations and oscillations are damped (Fig. 1, stage 1). Therefore, a system is needed to provide initial stability for the spacecraft to prevent a high angular acceleration of cargo after opening the parachute. Moreover, stable flight during final stages of mission will help more accurate and comfortable landing and recovery that is an important requirement especially for manned reentry vehicles.
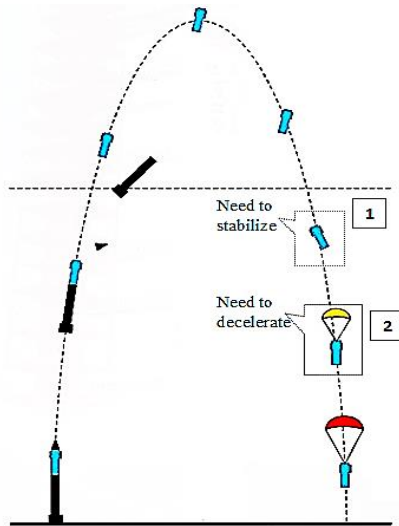

Fig. 1. Sub-orbital Re-entry Capsule in launch and descent process.

The performance of strips for providing stability primarily relates to the creation of force and the aerodynamic moments at the end of the body, and thus the production of an optimum moment for the dynamic stability of the body. Concerning the design goals and missionary, geometric and mass constraints presented as input to the design problem, several analyzes are required to optimize the design parameters. The computational cost of every three-dimensional analysis, which involves the unsteady simulation of body-fluid-structure interaction, is very high. Therefore, we need to use an optimal approach to the computational analysis process. In this study, a multi-disciplinary design consists of fluid solving, structure analysis and body oscillation is considered. So the complicated coupling of these disciplines needs a suitable framework to handle the problem and capture the nature of body-fluid-structure interactions, properly. Some related researches and studies about this issue are presented in the following.

Levine and Dasser (1997) conducted an experimental study on the characteristics of ribbons in the subsonic wind tunnel. This study was carried out based on the variation of the aspect ratio and rectangular ribbon material. Auman and Dalek (2000), Aumon and Wilkes (2005) and Lamar and Wain (2011), conducted an empirical test to determine the aerodynamic characteristics of ribbon stabilizers. Wang *et al.* (2012), used numerical solutions (imaginary field method) for three-

dimensional page movement. In one related study, Gomes and Leinheart (2013), used and combined commercial software to investigate body-fluid-structure interactions in the water that have got good results compared to empirical testing. Xiao and Wang (2016), gave a numerical simulation of the vortex-induced vibrations of vertical raisers in linear and uniform shear flows, and the predicted numerical results are in good agreement with experimental results. Dobrucali and Kinase (2017), in their paper about the prediction of vortex-induced vibration for circular cylinders using URANS have concluded that vibration caused by vortex due to three different frequencies is highly nonlinear: the frequency of the flow, the frequency of vortex fluctuation and the frequency of oscillation. Stabile *et al.* (2018), have also developed a reduced order modeling for the analysis of flexible long cylinders.

In the field of design of experiments (DOE) for aerospace applications, Tucker *et al.* (2010), used DOE methodology to a flight test. In this limited effort, an actual flight test program serves as a case study to compare and contrast five different designs to explore a flight-test envelope. Liang *et al.* (2016), applied Taguchi method for evaluating the maximum swimming speed of robotic fish under the limitation of the output of the motor. Four factors were considered in the optimization: the caudal-fin aspect ratio, the caudal fin stiffness, the oscillating frequency and the stiffness of the spring that transmits forces from the actuators to the foil. In another study, an empirical drag prediction model plus the design of an experiment, response surface, and data-fusion methods are brought together with computational fluid dynamics (CFD) to provide a wing optimization system. This system allows high-quality designs to be found using a full three-dimensional CFD code without the expense of direct searches (Keane, 2003). Lee and Jonathan (2016), presented an alternative formal methodology for smart weapons conceptual airframe design and optimization based on DOE. Khoshdast *et al.* (2017), combined two methods of CFD and DOE to hydrodynamic simulation of a coal classifier. Raul *et al.* (2017), used Design of Experiments and surrogate models in aircraft real-time and many-query aerodynamic analysis. Julian *et al.* (2017), applied design of experiments techniques to improve the thermal performance of a gas oven, aided with a computational fluid dynamics in concept selection phase of product design process.

In the present work, a hybrid approach, including computer code development and simultaneous use of existing solvers' capabilities, is adapted to simulate the complex problem of strip stabilizer oscillations attached to the trailing edge of a reentry space capsule, i.e. body-fluid-structure interactions. Expected achievements can be summarized as: 1) Developing a suitable computational framework for analyzing body-fluid-structure interactions. 2) Dynamic analysis of rigid body with a flexible strip stabilizer attached to its trailing edge. 3) Modification of the stabilizer design process and sensitivity analysis using Design of Experiments. 4)

Design of flexible stabilizer, based on the results of aero-elastic analyses. The main features of the presented work are, three-dimensionality of the solution, emphasize on the stabilization process, and developing an iterative partitioned framework for Body-Fluid-Structure interaction (BFSI) analysis. Moreover, through implementing DOE technique we tried to manage the computational cost. The results of the present work are useful for any flying vehicle which needs to stabilize e.g. before opening the parachute during descent phase or when some limitations exist on the minimum angular acceleration inserted on the sensitive payload i.e. living organisms.

2. GOVERNING EQUATIONS

2.1 Fluid flow Equations

The governing equations for fluid flow are Navier-Stokes equations, which are defined as below:

a- *Continuity equation*

$$\frac{\partial \rho}{\partial t} + \frac{\partial}{\partial x_j}\left(\rho U_j\right) = 0 \tag{1}$$

b- *Momentum equation*

$$\frac{\partial \rho U_i}{\partial t} + \frac{\partial}{\partial x_j}\left(\rho U_i U_j\right) = -\frac{\partial p'}{\partial x_i} +$$
$$\frac{\partial}{\partial x_j}\left[\mu_{eff}\left(\frac{\partial U_i}{\partial x_j} + \frac{\partial U_j}{\partial x_i}\right)\right] \tag{2}$$

In order to solve these equations in viscous fluid mode and high Reynolds numbers, a turbulent modeling is needed, where the *k-ε* model is used here. In this model, the concept of the viscosity of vortex is used:

$$\mu_{eff} = \mu + \mu_t \tag{3}$$

The vortex viscosity is defined as follows:

$$\mu_t = C_\mu \rho \frac{k^2}{\varepsilon} \tag{4}$$

And the partial transmission equations for turbulent kinetic energy and disturbance dissipation rate are as follows:

$$\frac{\partial(\rho k)}{\partial t} + \frac{\partial}{\partial x_j}\left(\rho U_j k\right) = \frac{\partial}{\partial x_j}\left[\left(\mu + \frac{\mu_t}{\sigma_k}\right)\frac{\partial k}{\partial x_j}\right] +$$
$$P_k - \rho\varepsilon + P_{kb} \tag{5}$$

$$\frac{\partial(\rho\varepsilon)}{\partial t} + \frac{\partial}{\partial x_j}\left(\rho U_j \varepsilon\right) = \frac{\partial}{\partial x_j}\left[\left(\mu + \frac{\mu_t}{\sigma_\varepsilon}\right)\frac{\partial \varepsilon}{\partial x_j}\right] +$$
$$\frac{\varepsilon}{k}\left(C_{\varepsilon 1}P_k - C_{\varepsilon 2}\rho\varepsilon + C_{\varepsilon 1}P_{\varepsilon b}\right) \tag{6}$$

Where P_k is the force of turbulence due to the viscous forces:

$$P_k = \mu_t\left(\frac{\partial U_i}{\partial x_j} + \frac{\partial U_j}{\partial x_i}\right)\frac{\partial U_i}{\partial x_j} - \frac{2}{3}\frac{\partial U_k}{\partial x_k}\left(3\mu_t\frac{\partial U_k}{\partial x_k} + \rho k\right) \tag{7}$$

2.2 Flexible Structure Equations

Considering the fact that the strip is considered thin, with a low width and the type of connection (clamped) to the body is such that its main oscillations are in the *xy* plane, such as a cantilevered beam with a distribution of extensive load we obtain the relation of Euler-Bernoulli beam. The transverse motion equation under the extensive transverse force is:

$$\frac{\partial^2}{\partial x^2}\left[EI(x)\frac{\partial^2 w(x,t)}{\partial x^2}\right] + \rho A(x)\frac{\partial^2 w(x,t)}{\partial t^2} = f(x,t) \tag{8}$$

Using the method of natural modal analysis, the above relation solution is obtained by linear combination of natural modes of the beam as follows:

$$w(x,t) = \sum_{i=0}^{\infty} W_i(x)\eta_t(t) \tag{9}$$

Where η_t is the generalized coordinates and W_i is natural modals that are obtained by solving the following equation:

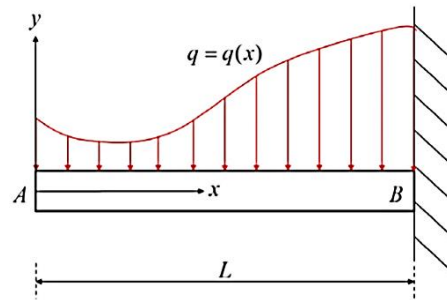$$\frac{d^2}{dx^2}\left[EI(x)\frac{d^2 W_i(x)}{dx^2}\right] - \rho A(x)\omega_i^2 W_i(x) = 0 \tag{10}$$

Fig. 2. Distribution of extensive load on cantilever beam.

Then we have:

$$\sum_{i=1}^{\infty}\frac{d^2}{dx^2}\left[EI(x)\frac{d^2 W_i(x)}{dx^2}\right]\eta_t(t) +$$
$$\rho A(x)\sum_{i=0}^{\infty}W_i(x)\frac{d^2\eta_i(t)}{dt^2} = f(x,t) \tag{11}$$

After substituting the above equations:

$$\sum_{i=1}^{\infty} \eta_t\left(t\right) \int_0^1 \rho A\left(x\right) \omega_i^2 W_j\left(x\right) W_i\left(x\right) dx +$$

$$\sum_{i=1}^{\infty} \frac{d^2 \eta_i\left(t\right)}{dt^2} \int_0^1 \rho A\left(x\right) W_j\left(x\right) W_i\left(x\right) dx = \quad (12)$$

$$\int_0^1 W_j\left(x\right) f\left(x,t\right) dx$$

According to the condition of orthogonally, all the terms on the left of the above relationship are deleted except for the case $i = j$. Then we have:

$$\frac{d^2 \eta_i\left(t\right)}{dt^2} + \omega_i^2 \eta_i\left(t\right) = Q_i\left(t\right), \quad i = 1, 2, \ldots \quad (13)$$

Where Q_i *(t)* is the generalized force, and for i_m mode, it is:

$$Q_i\left(t\right) = \int_0^1 W_i\left(x\right) f\left(x,t\right) dx, \quad i = 1, 2, \ldots \quad (14)$$

The complete solution of the relationship can be expressed as follows:

$$\eta_i\left(t\right) = A_i \cos \omega_i t + B_i \sin \omega_i t +$$

$$\frac{1}{\omega_i} \int_0^t Q_i\left(\tau\right) \sin \omega_i\left(t - \tau\right) d\tau \quad (15)$$

Therefore, the final relation for Euler-Bernoulli beam is as follows:

$$w\left(x,t\right) = \sum_{i=1}^{\infty} \left[A_i \cos \omega_i t + B_i \sin \omega_i t + \right.$$

$$\left. \frac{1}{\omega_i} \int_0^t Q_i\left(\tau\right) \sin \omega_i\left(t - \tau\right) d\tau \right] W_i\left(x\right) \quad (16)$$

The first two expressions represent free oscillation and the third term indicates the forced oscillation of the beam. A_i and B_i are fixed numbers and also are obtained using the initial conditions.

2.3 Rigid Body Dynamic Model

To simulate the dynamic of body, following equations are used. It is noticeable that moments are considered about the body center of mass.

The equations of forces exerted on stabilizer concerning Fig. 3 (up) are determined as follows:

$$\begin{cases} F_x = \sum_{i=1}^{n} \left[P_i\left(A_x\right)_i + \tau_i\left(A_y\right)_i \right] \\ F_y = \sum_{i=1}^{n} \left[P_i\left(A_y\right)_i + \tau_i\left(A_x\right)_i \right] \end{cases} \quad (17)$$

Where F_x is axial force, F_y is normal force, P_i is fluid pressure on surface element, τ_i is shear stress on surface element, A_x is projection of surface element on longitudinal direction, A_y is projection of surface element on transverse direction and i is the number of elements.

The forces imposed on the body from the fluid around it are obtained from Eqs. 17 on body elements. The equation of moment exerted on body from the fluid around it, is as follows:

$$M_{Body} = \sum_{i=1}^{n} \left(\left[P_i\left(A_x\right)_i + \tau_i\left(A_y\right)_i \right] y_i + \right.$$

$$\left. \left[P_i\left(A_y\right)_i + \tau_i\left(A_x\right)_i \right] x_i \right) \quad (18)$$
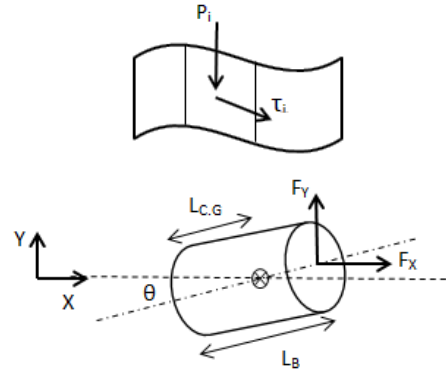

Fig. 3. Pressure and shear stress on an element of structure (up) and inserted forces on body from stabilizer (down).

The equation of moment exerted on body from stabilizer concerning Fig. 3 (down) is as follows:

$$M_{Stablizer} = F_{x_{Stab}} * \left(L_B - L_{C.G}\right) \sin\left(\theta\right) + \quad (19)$$

$$F_{y_{Stab}} * \left(L_B - L_{C.G}\right) \cos\left(\theta\right)$$

where $F_{x_{Stab}}$ and $F_{y_{Stab}}$ are respectively, axial and normal forces exerted on body from the stabilizer in the contact point, L_B is body length, $L_{C.G}$ is the distance of body center of mass from its tip and θ is the angle of body longitudinal axis from horizon. Finally from relations (18) and (19) total moment for body stabilizing is obtained from the equation:

$$M_{Total} = M_{Body} + M_{Stablizer} \quad (20)$$

2.4 Analysis Model of (DOE)

In this work, Taguchi model is implemented for the design of experiments. Taguchi used the following models to achieve the expected results:

- Analysis of variance (ANOVA)

- Signal to noise ratios (S/N)

Taguchi defined S/N ratio differently according to the quality characteristic, i.e., the-lower-the-better, the-nominal-the-better, and the-higher-the-better, which their relations respectively are as follows:

$$\left(S/N\right)_l = -10\log\left(\frac{1}{n} \sum_{i=1}^{n} y_i^2\right) \quad (21)$$

$$\left(S/N\right)_n = -10\log\left[\frac{1}{n} \sum_{i=1}^{n} \left(y_i - y_0\right)^2\right] \quad (22)$$

$$\left(S/N\right)_h = -10\log\left(\frac{1}{n} \sum_{i=1}^{n} \frac{1}{y_i^2}\right) \quad (23)$$

Where n is the test number, y_i is the trial result of

*i*th test and y_0 is the nominal value. Various models used to analyze the results of the design of experiments methods are as follows:

-Linear:

$$y = \beta_0 + \sum_{i=1}^{k} \beta_i x_i \qquad (24)$$

- Linear Concerning Binary Interactions (2FI):

$$y = \beta_0 + \sum_{i=1}^{k} \beta_i x_i + \sum \sum_{i<j} \beta_{ij} x_i x_j \qquad (25)$$

-Quadratic:

$$y = \beta_0 + \sum_{i=1}^{k} \beta_i x_i + \sum \sum_{i<j} \beta_{ij} x_i x_j$$
$$+ \sum_{i=1}^{k} \beta_{ii} x_i^2 + \epsilon \qquad (26)$$

where *y* is the desired index, β_0 is the nominal value of the index, β_i is the slope of the line of variation of the variable (constant number) and x_i is the desired variable such as length, width, mass...

2.5 Algorithm of Fluid-Structure Interaction

In order to analyze the fluid-structure interaction, an algorithm must be available to solve the structure and fluid equations simultaneously (monolithic method) or to establish a logical relationship between the results of the solution of the fluid equations and the structures (partitioned method). Also, it can adapt fluid and structure grids if they are not the same. The first method is very time-consuming, expensive and not affordable. In the second method, the fluid-structure equations are solved with separate solvers that can even be non-editable (black box), and their results are exchanged with a combined algorithm. This method makes it possible to use a variety of solvents and has high flexibility. The partitioned method is applicable in two ways, as shown in Fig. 4.

In the first method (Fig. 4, up), called a staggered (parallel staggered) method, at every time step, the fluid-structure data are exchanged, and then the equations are solved simultaneously but independently. In the second method (Fig. 4, down), which is called iterative (serial staggered) method, the fluid equations are solved first, and then the data are entered into the structural part and the structure equations are solved based on the new information of the fluid and its data are fed into the fluid section. The fluid equations are again solved based on the new structure data and this repeating cycle continues until the problem is completely solved. In this paper, the iterative partitioned coupling algorithm is used.

From the perspective of the type of coupling algorithm, we can say that there are two types that include a weak coupling algorithm and a strong or precise coupling algorithm. In a weak coupling algorithm at any time step, we have only one solution of the structure and fluid. Therefore, it is needed to take a fine and empirically time step, otherwise, the solution divergence will occur. But in a strong coupling algorithm at any time step, we have several solutions of the fluid and structure equations that are fully synchronized and the aeroelastic system be converged. Therefore, the solution is prolonged (strong algorithm), but it is much more stable than the previous one (weak algorithm). In addition, it is algorithmically flexible and applicable to various physical systems.
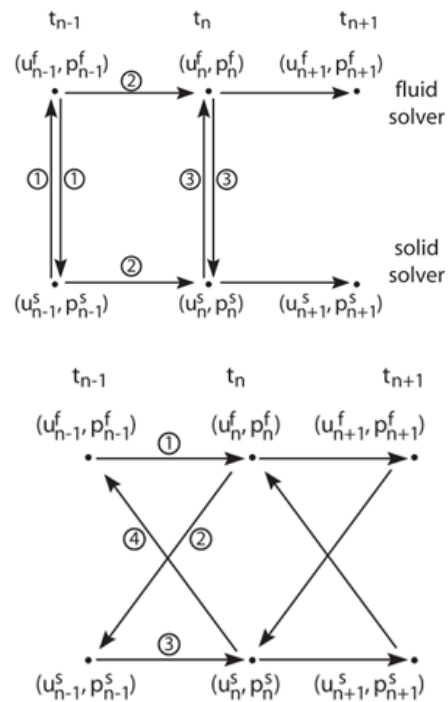

Fig. 4. Schematic of staggered (up) and iterative (down) methods.

The flowchart of the iterative partitioned coupling algorithm used in this paper is shown in Fig. 5. The process of analysis is that, at first by solving the flow equations, the distribution of pressure is determined around the body and the forces and moments imposed on it, are determined. Then, using the equations of rigid body dynamics and according to the distribution of the pressure and the forces applied to the body, the new state of the body is determined. Now, using structural equations, structural deformation is calculated and then new calculated points are updated. Then due to the new coordinates of the structure, re-meshing technic is performed and concerning new grid, fluid equations are solved. In the next step, solution convergence is checked out and if approved, moves to the next time step. This process continues until the criterion of the end of the process is fulfilled. After analyzing body-fluid-structure interaction, considering the results and on the basis of DOE methodology, the design process starts. In Fig. 6, the algorithm of the design of experiment process is shown.
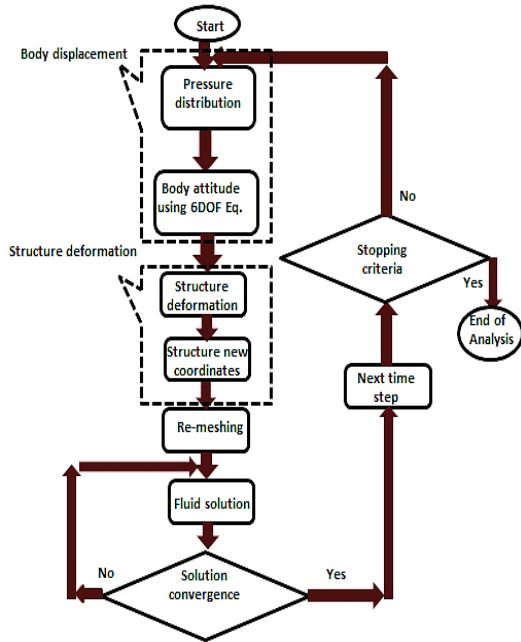
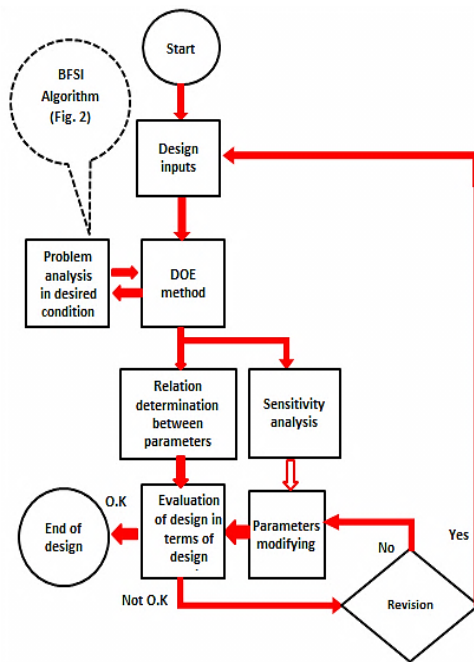**Fig. 5. Coupling algorithm of solution of the body-fluid-structure interaction problem.**

Fig. 6. Algorithm of DOE process.

3. STATEMENT OF PROBLEM AND MODEL

As many other related works, we have used a commercial software (Fluent) for the analysis of fluid flow part of the FSI problem, to focus mainly on the fluid-structure interaction simulation. Thus, we have written a user defined functions (UDF) code for structure analysis, based on the Euler-Bernoulli cantilevered beam theory and iterative partitioned coupling algorithm.

3.1 Geometry and Fluid Domain Condition

A three-dimensional cylinder simplified geometry of Fig. 1, with a strip (flexible thin plate), connected to its end, is intended to investigate the problem of fluid-structure interaction. It is noticeable that the details of geometry in Fig. 1 are not vital for the analysis and it was shown only as a sample of application in aerospace industry. The simplified geometry of the body and strip is shown in Fig. 7. The aim is to analyze the stability of body in the last phase of trajectory (decent) which is near the earth surface. So, flow Mach number is set 0.4 and the density of fluid in this conditions is nearly constant about 1.16 kg/m^3.
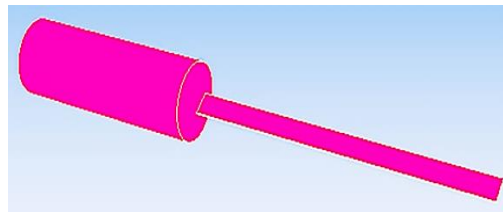

Fig. 7. Body and strip scheme.

3.2 Grid Study

a- Body and Fluid Domain Grid

Concerning that fluid flow analysis is in an unsteady state and the motion of the body and strip cause the grid of fluid domain to collapse, the moving mesh and re-meshing are used at any time step. Because the geometry and the angles of cells are changed at any instant and are collapsed, therefore using unstructured mesh is better and more appropriate than structured mesh.

However, because the body is rigid and only rotates, and in addition, the grid of strip does not collapse; as a result, the structured mesh is used for both of them. In Fig. 8, the grids of the body with strip and domain are presented.
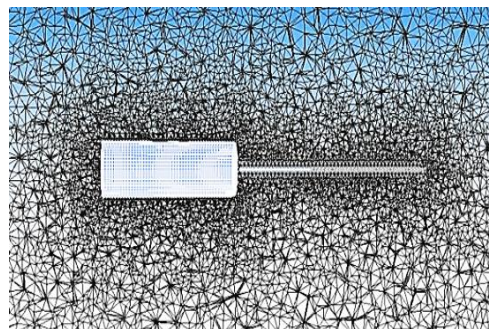

Fig. 8. Body and strip grids (structured) and fluid domain grid (unstructured).

In order to ensure the accuracy of the analysis and the independence of the results to the number of grid cells, some grids with different cell numbers were modeled which the numbers of cells were 80000, 130000, 340000, 600000 and 780000

cells. In Fig. 9, the pitching moment coefficient is plotted versus the number of cells for each grid. It was found that for a model with 330000 cells, the pitching moment coefficient differs about 3% compared with the 780000 cells model, which is negligible, and since the model with 340000 cells takes less computational time than the model with 780000 cells, so it was used for next analysis.
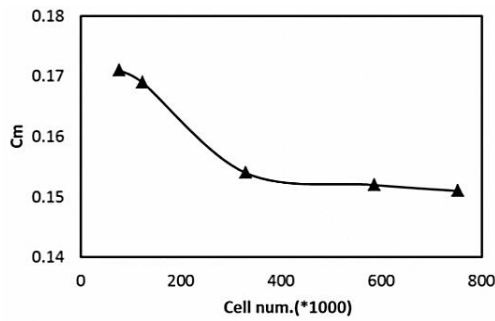

Fig. 9. Pitching moment coefficient versus grid cell numbers.

b- *Flexible Structure Grid*

In the following, we investigate the independence of the results to the number of cells in the grid of strip. For this purpose, differently structured meshes with the different number of cells were considered. Five grids with 246, 326, 406, 486 and 566 cells were created and according to the application of the problem, in Fig. 10, pitching moment coefficient is plotted based on the numbers of grid cells and it was found that the model, which has 406 cells, has a difference of about 2% compared with the 566 cells model, which is negligible and therefore, considering the computational cost, the same grid was selected for further analysis. In Fig. 11, a structured grid for the strip is shown.
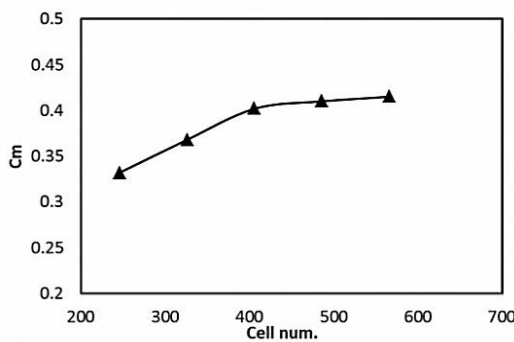

Fig. 10. Pitching moment coefficient versus grids cells number.

4. RESULTS AND DISCUSSIONS

At first, for the validation of the developed code, we analyzed an elastic plate as a cantilevered beam attached to the end of a square, as considered in the work of Hubner *et al.* (2004). The dimensions of geometry and surrounding domain are presented in

Fig. 12. A snapshot of pressure contours around the body and its trailing edge stabilizer is shown in Fig. 13. Also, the transverse force of plate is compared with the reference work in Fig. 14. The results of simulations indicate good agreement between the present work results and reference data.
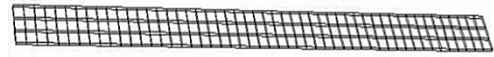

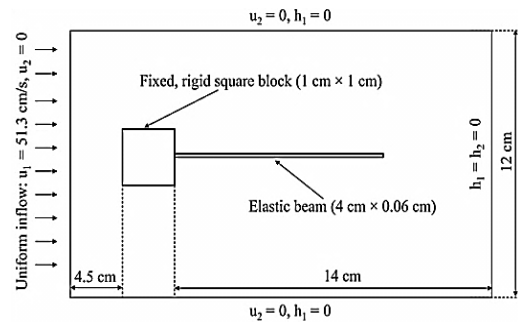**Fig. 11. Structured grid for the flexible strip.**

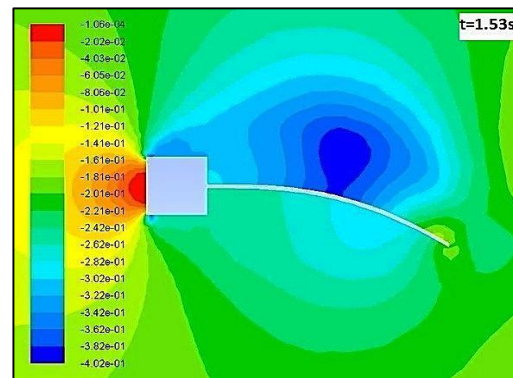**Fig. 12. Geometry and domain of the test case.**

Fig. 13. Pressure Contours around the test case.
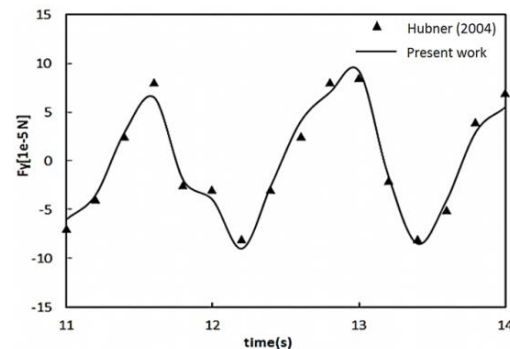

Fig. 14. Comparing of transverse force of plate with the results of Hubner *et al.* (2004).

In the remain of this section, note that for all investigations, Mach number is 0.4 and the angle of attack is 10 degrees as they encountered in the targeted phase of flight envelope.

4.1 Setting Initial Condition

In this investigation, the finite volume method is used to solve the fluid flow. Since the flow conditions are within the compressible range, here a density-based algorithm is used to associate the equations. Time discretization is performed implicitly. The standard k-ε model is used for modeling the turbulent flow. The second-order accuracy has been used for spatial discretization, and the gradients have been calculated based on the least squares of the cell base.

4.2 Effect of the Strip on Body Oscillations and Aerodynamic Coefficients

In Fig. 15, the oscillations of the body alone and body with strip are presented. The angle of the body alone is increased gradually because it is unstable inherently. However, when the strip is added to the end of the body, it prevents from increasing the amplitude of oscillation by creating a restoring moment and body has a periodic (stable) oscillation about a small angle. In Fig. 16, axial and normal forces due to strip oscillations are shown.
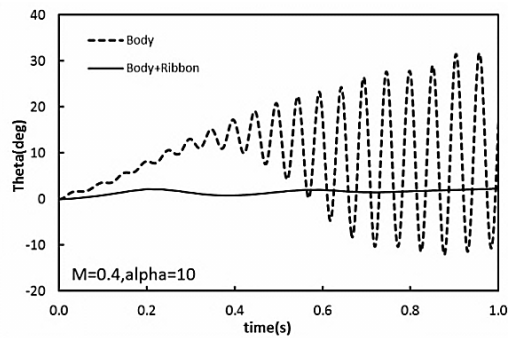

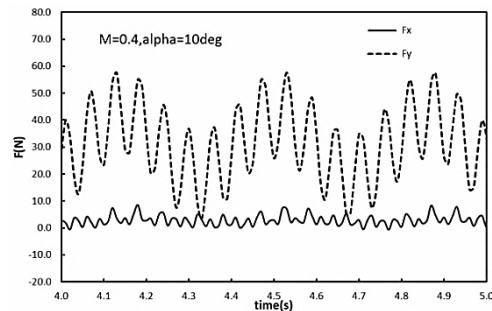Fig. 15. Oscillations of the body with and without strip versus time.

Fig. 16. Axial and normal forces of oscillating strip versus time.

In the following, the effect of strip on aerodynamic coefficients of the body is presented. Table 1 shows the aerodynamic coefficients of a body alone and with the strip in the static state which presents that the maximum effect of the strip is on the normal force and the presence of a strip at the end of body can have a significant effect on the aerodynamic coefficients even in static state. In Figs. 17, Mach number contours on the body and strip in different instants are presented that show the deformations of strip attached to the free oscillating body.

Table 1 Aerodynamic coefficients for the static body with and without the strip

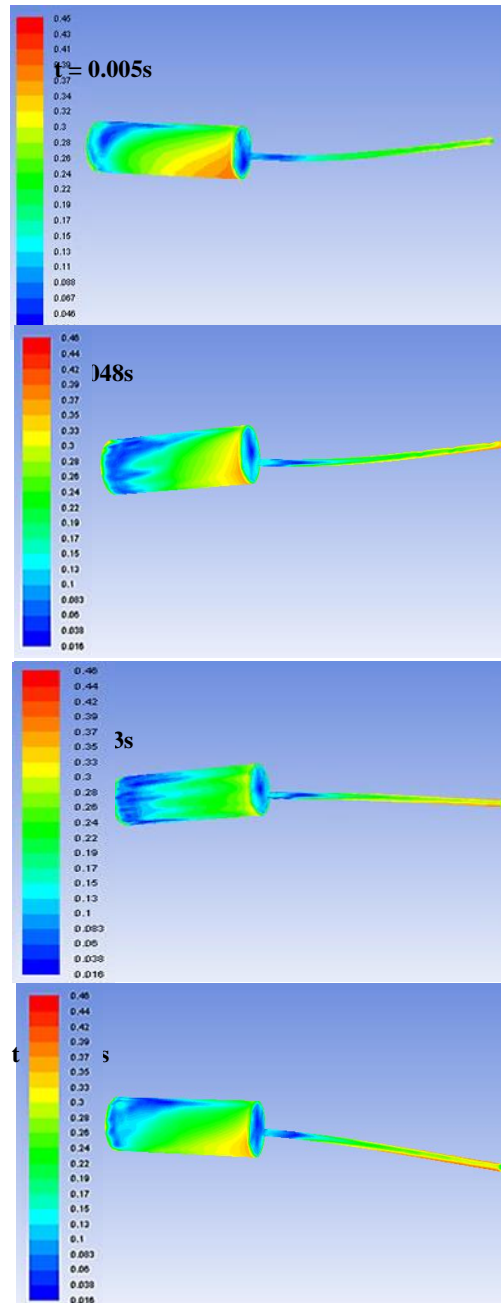| Aerodynamic coefficients	Body alone	Body with strip
C_a	1.04	1.35
C_n	0.11	0.41
C_m	-0.08	-0.11

Fig. 17. Mach contours on the body/strip surface.

4.3 Effect of the Body Center of Mass

Concerning that the location of the body center of mass affects its oscillations, two locations were considered for body center of mass that one of them is in Xcg=0.15m and the other one is in

Xcg=0.1m from body leading edge. The results of the investigation are presented in Fig. 18.

It can be concluded from Fig. 18 that the oscillation frequency and amplitude of the body increase if the center of mass goes backward, which is expectable based on stability conditions. Of course, it is noteworthy, this type of geometry is inherently unstable and c.g. displacement is not a solution to its instability duo to the configuration constraints. Also, the oscillation intensity is higher when the center of mass is more backward and as a result, if there is a payload that is sensitive to the angular accelerations, its failure is more probable.
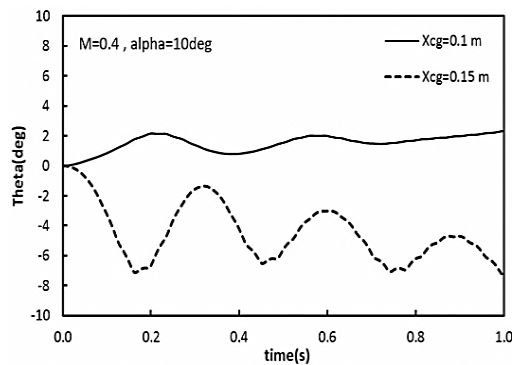

Fig. 18. Body oscillation angle versus time for different body center of masses.

4.4 Effect of Length and width of the Strip

In the following, we studied variations of strip length for two different lengths consist of 0.5L and 1.5L which L is the length of ribbon. The angle of body oscillation in Fig. 19 is presented for the above-mentioned strip lengths. As can be seen, more length of strip prevents from a large oscillation angle of the body. In Fig. 20, the body oscillation angle versus time for different width of strip is presented that same result can be concluded.
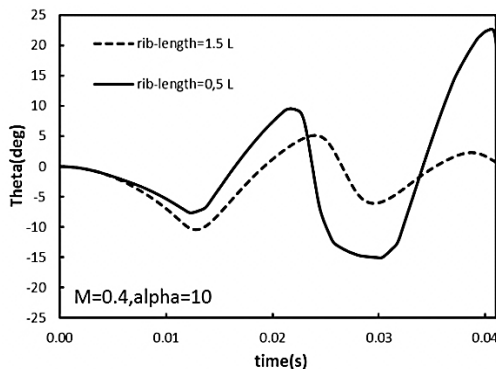

Fig. 19. Body oscillation angle versus time for different length of the strip.

4.5 Effect of flow Velocity (Mach Number)

In this section, by assuming that the center of

mass is in front of the body, the effect of flow velocity on the body oscillations is investigated. The results of this study are presented in Fig. 21. As can be seen, with the increase of Mach number, the amplitude of strip oscillations decreases but the frequency is increased, so for a sensible cargo, it may cause to damage or fail. Therefore in the main phase of the flight path of this vehicle which Mach number is about 0.4, the payload is almost safe and there will be not any dangerous condition.
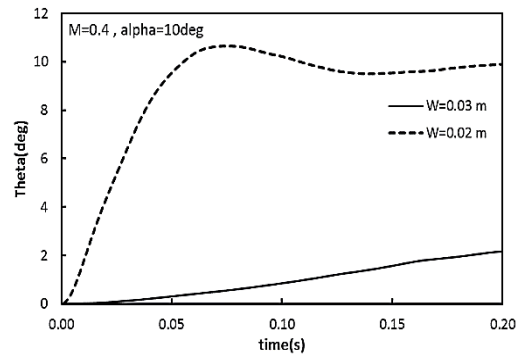

Fig. 20. Body oscillation angle versus time for different width of the strip.
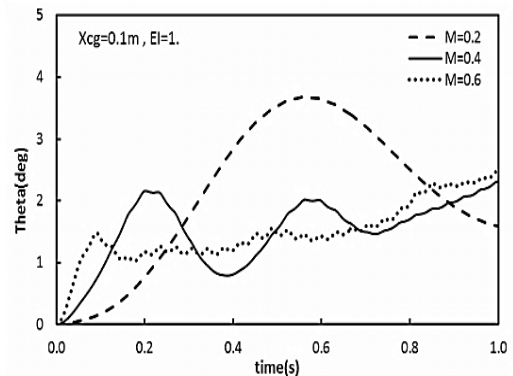

Fig. 21. Body oscillation angle versus time in different Mach number.

4.6 Computational Efficiency

Initially, the average duration of each analysis is presented in order to examine and compare the computational efficiency in two-dimensional, three-dimensional, static and dynamic states, with or without strip (Tables 2 and 3). A numerical solution is performed using a laptop with Intel Core i5 processor 2.1 GHz. As can be seen, for numerical computations of fluid-structure interaction in the three-dimensional case and with concerning oscillations of body and flexible strip attached to it, it takes about two hours. It should be noted that according to the type of problem, the two-dimensional analysis is presented only for comparison, and it is obvious that the three-dimensional state must be taken into account for the correct analysis of the problem.

Table 2 Average duration of numerical computation for the body alone

3-dimensional		2-dimensional		
Dynamic	Static	Dynamic	Static	
98	79	58	21	time (minutes)

Table 3 Average duration of numerical computation for the body with strip

3-dimensional		2-dimensional		
Dynamic	Static	Dynamic	Static	
112	85	64	24	time (minutes)

5. DESIGN OF STRIP USING DOE

Now, after various analysis and computational efforts performed in different flight conditions, the desired design is captured based on obtained results, by using an efficient and suitable method which a strip can be designed to meet the designer's requirements and expectations. In the following, the design process is presented using the obtained results and DOE methodology, which can be an important step for appropriate design (or even optimizing) of the strip with consumption of minimal time and cost. Two usual methods for DOE implementation are Full Factorial (FF) and Taguchi methods. For low variables and parameters, the Full Factorial method is better than Taguchi method. Because it determines possible factors interactions and is simpler than Taguchi method for performing, but for several variables and parameters, Taguchi method is better, because uses orthogonal arrays and considerably reduces the number of experiments and cost. So in this paper, concerning that we have three variables in two levels, the Full Factorial method with 23=8 experiments is used.

Variables that can be considered for the strip consist of length, width, thickness, and bending stiffness, and the variables of the oscillating rigid body consist of the body center of mass, length, and radius. It should be noted that due to some our design constraints, we only consider the parameters of length and width of the strip and body center of mass in two levels and analyze the design of a sample, based on the variations of three parameters.

In the following, the variation in the length and width of the strip is considered to be 20% of its nominal values. So for parameters values less than the nominal value the number -1 is assigned and for parameters values more than the nominal value the number +1 is assigned. For this purpose, the values of the strip width are 0.016 (-1) and 0.024 meters (+1), and for the length of the strips are 0.36 (-1) and 0.54 meters (+1) and finally for body center of mass are 0.08 (-1) and 0.12 meters (+1). The values of design

parameters and assigns of them are presented in Tables 5 and 6. In Figs. 22 and 23 the slope of parameters variations and their interactions are presented and in Fig. 24, the Pareto chart is presented. In Pareto chart the most important of variables are determined. In Fig. 25 the contribution percent of all factors to the model is determined. Using the results of Figs. 24 and 25, important variables for design are specified.

After performing the necessary changes to the variables, the line slopes of variations of parameters are presented in Table 4. Finally, concerning the above analyzes, the maximum angle of body oscillation will be as follows:

$$\theta = 6.8 - 3.24L_r - 1.7W_r + 2.8X_{CG} - \qquad (27)$$
$$1.48L_rX_{CG} + 0.48L_rW_r -$$
$$0.76W_rX_{CG} + 0.6L_rW_rX_{CG}$$

Relation 27 determines the value of maximum oscillation angle of body for various lengths and widths of the strip and body center of mass in the range of 20% deviation from the nominal value.
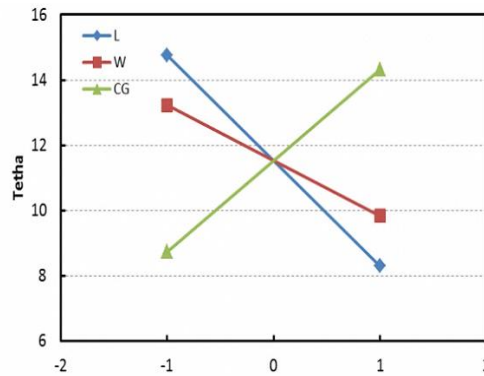

Fig. 22. Body oscillation angle versus variations of length, width, and the body center of mass.
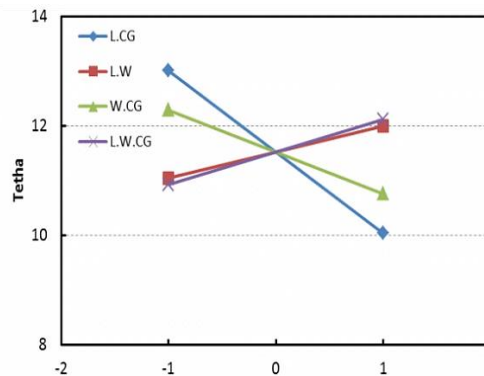

Fig. 23. Body oscillation angle versus the interactions of variables.

5.1 Verification of DOE Results

We consider a strip with a length of 0.4 m, a width of 0.022 m and the body center of mass, 0.1 m (within the range of changes from nominal

values), and use two manner for calculation of the maximum angle of oscillating body. For the first method, we simulate and analyze the problem and for the second method, we use relation 27 to calculate the body maximum angle. The results are as follows:

Angle (from simulation) $\theta = -7.04^\circ$

Angle (from relation 27) $\theta = -7.8^\circ$

As can be seen from the comparison of results, the oscillation angle obtained from relation 27 is less than 11% different from what obtained from the simulations, which is acceptable and verifiable.
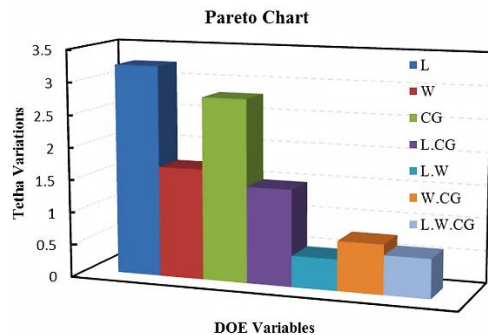
Table 5 Parameters values considering length and width in two levels

L (m)	W (m)	CG (m)	θ
0.54	0.024	0.12	15.5
0.54	0.024	0.08	9.67
0.54	0.016	0.12	22.58
0.54	0.016	0.08	11.29
0.36	0.024	0.12	8.21
0.36	0.024	0.08	5.92
0.36	0.016	0.12	11.0
0.36	0.016	0.08	8.04
Nominal values (*L*=0.45 m, *W*=0.02 m, *CG*=0.1 m)			6.8

Fig. 24. Pareto chart for the oscillation angle variation versus variations of length, width, and their interaction.
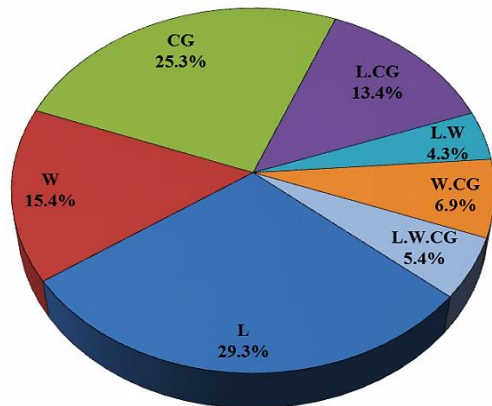

Fig. 25. Contributions of variables to the model.

Table 4 The line slopes of the variations of the parameters

Parameter	Line Slope
L (Length)	-3.24
W (Width)	-1.7
CG (body mass center)	2.8
L.CG	-1.48
L.W	0.48
W.CG	-0.76
L.W.CG	0.6

Therefore, by using this method (DOE), it is simple to examine the changes in geometric parameters and their effects on the oscillatory characteristics of the body such as the instant angle of oscillation, at least cost and time. Therefore, it doesn't need extensive simulations and time consuming computational runs. It is noteworthy that it's better to have less change within the range of the parameters variation comparing with nominal values (length, width, and ....) to minimize the error of the calculations results.

In the following, for example, we compute the maximum desired body oscillation angle. Suppose that the maximum desired angle of body oscillation is 0 degree and body center of mass is 0.14 m and the width of the strip is 0.02 m. it is noticeable that the converted (assigned) values of factors are inserted in the relation (on the basis of -1 and +1) so at first, we must convert the values in this range then insert in the relation. Now, we want to determine the length of the strip that supports the desired oscillation angle. Using relation 27 and substituting the specified values, the length of the strip will be 0.63 m. As can be seen, other factors could be easily determined for any change in the desired performance characteristics.

5.2 DOE Computational Efficiency

All numerical computations is performed using a Laptop with Intel Corei5 CPU (2.1 GHz frequency). For every computational run, it takes about 112 minutes. So, for this case with 8 runs, it takes about 900 minutes. But we have captured a relation that helps to determine the instant oscillation angle easily and timely. But, for any change in geometry if we don't use the DOE method and we simulate and run all of the cases, then we must spend a lot of time and cost to calculate the oscillation angle and finally we can't recognize a proper geometry consist of length and width. Therefore we won't have a proper and efficient design. So this initial investment causes to save time and computational costs. These results are presented in Table 5. Where, OFAT is an acronym for "one factor at a time" that means it will be necessary performing many computational efforts of the direct search on the CFD code, which at any effort only one parameter varies. So with using the DOE method, the time is saved 60% at least and the design

Table 6 Parameter values considering length and width in two levels

L	W	CG	L.W	L.CG	W.CG	L.W.CG	θ
+1	+1	+1	+1	+1	+1	+1	15.5
+1	+1	-1	+1	-1	-1	-1	9.67
+1	-1	+1	-1	+1	-1	-1	22.58
+1	-1	-1	-1	-1	+1	+1	11.29
-1	+1	+1	-1	-1	+1	-1	8.21
-1	+1	-1	-1	+1	-1	+1	5.92
-1	-1	+1	+1	-1	-1	+1	11.0
-1	-1	-1	+1	+1	+1	-1	8.04

process uses around one-third of the direct search on CFD code.

Table 7 Computational time saving with DOE for three factors in two levels

Number of runs	Run duration(min)
1	112
8 (using DOE)	900
several (using OFAT)	high

6. CONCLUSIONS

Numerical analysis of free body oscillations with a trailing edge flexible stabilizer was done in viscous subsonic flow regime. For fluid flow simulation, finite volume method was used and for structural analysis Euler-Bernoulli cantilevered beam theory was implemented. For the fluid-structure interaction solution, iterative partitioned coupling algorithm was used for interrelation.

Combining a dynamics simulation tool the proposed computational framework is capable to capture the Body-Fluid-Structure interactions. The results of different simulations shows that without the flexible stabilizer, the oscillations of free flying body will grow towards instability. In order to analyze the Body-Fluid-Structure interaction, a computational framework based on an iterative partitioned coupling algorithm was developed which the results showed the capability of capturing the physics of this complicated problem.

Also, using the developed tool, the impact of important parameters were examined which was shown that as the body center of mass moves to forward (toward the body tip), the body oscillation amplitude and frequency decrease. Likewise, with increasing flow velocity (Mach number), the amplitude of the body oscillation decreases and the frequency increases. Finally, for the design of a suitable stabilizing strip, the DOE methodology was used. For low variables and parameters, the Full Factorial method was better than the Taguchi method. Because it determines possible factors interactions and is simpler than Taguchi method.

REFERENCES

Tucker A. A., G. T. Hutto, C. H. Dagli, (2010). Application of design of experiments to flight test: a case study. *Journal of aircraft* 47(2).

Auman, L. M. and B. L. Wilks (2005). Application of Fabric Ribbons for Drag and Stabilization. *Aerodynamic decelerator systems technology conference and seminar, AIAA 2005*-1618.

Auman, C., M. Lamar, W. Dahlke (2000). Aerodynamic characteristics of ribbon stabilized grenades, *38th aerospace sciences meeting and exhibit, AIAA*-2000-270.

Dobrucali, E. and O. K. Kinaci (2017). URANS-Based Prediction of Vortex Induced Vibrations of Circular Cylinders. *Journal of applied fluid mechanics* 10(3), 957-970.

Gomes, J. P. and H. Leinhart (2013). Fluid-structure interaction-induced oscillation of flexible structures in laminar turbulent flows. *Journal of fluid mechanics* 715, 537-572.

Hubner, B., E. Walhorn and D. Dinkler (2004). a Monolithic Approach to Fluid-Structure Interaction Using Space-Time Finite Elements. *Journal of Computer Methods in Applied Mechanics and Engineering* 193, 2087-2104.

Julian, I., G. Ramiro, H. Paulo, E. Carlos and P. Anderson (2017). Improve the product design process, with CFD and DOE approach, *International Conference on Industrial engineering and Operations Management, Bogota, Colombia,* October 25-26.

Keane, A. J. (2003). Wing optimization using design of experiments response surface, data fusion methods. *Journal of aircraft* 40(4).

Khoshdast, H., V. Shojaei and K. Hami (2017). Combined application of computational fluid dynamics (CFD) and design of experiments (DOE) to hydrodynamics simulation of a coal classifier. *International Journal of mining and Geo engineering* 51(1), 9-22.

Lamar, M., C. Auman and W. Dahlke (2011). Drag Characteristics of Ribbons. *AIAA* 2001-2011.

Lee, F. and R. Jonathan (2016). Performance

optimization of guided projectiles using design of experiments. *AIAA Atmospheric Flight Mechanics Conference*, AIAA 2016-0540.

Levin, D., G. Daser and Z. Shpund (1997). On the Aerodynamic Drag of Ribbons. *AIAA*-97-1525.

Liang, Li, L. Jiang, C. Wang, W. Wei, Z. Xing and X. Guangming (2016). Application of Taguchi method in the optimization of swimming capability for robotic fish. *International Journal of advanced robotic systems 13,* 102.

Raul, Y., A. Esther and V. Eusebio (2017). A review on design of experiments and surrogate models in aircraft real-time and many-query aerodynamic analysis. *Journal of Progress in Aerospace Sciences 96,* 23-61.

Stabile, G., H. G. Matthies and C. Borri (2018). A novel reduced order model for vortex induced vibrations of long flexible cylinders. *Journal of Ocean Engineering 156,* 191-207.

Wang, Y., Z. Yu and X. Shao (2012). Numerical simulations of the flapping of a three-dimensional flexible plate in uniform flow. *Journal of Sound and Vibration* 331, 4448-4463.

Xiao, Q. and E Wang (2016). Numerical simulation of vortex-induced vibration of a vertical riser in uniform and linearly sheared currents. *journal of Ocean Engineering* 121, 492-515.